(2)

OFFICE OF NAVAL RESEARCH

CONTRACT N00014-84-k-0656/O00002

R & T Code 413d018

Technical Report #18

Variable Length-Scale Studies at Interfaces with X-ray Standing Waves

H.D. Abruña, G.M. Bommarito and D. Acevedo
Department of Chemistry
Baker Laboratory
Cornell University
Ithaca, New York 14853

Prepared for Publication in
SCIENCE
June 4, 1990

UNCLASSIFIED
SECURITY CLASSIFICATION OF THIS PAGE

REPORT DOCUMENTATION PAGE

1a. REPORT SECURITY CLASSIFICATION unclassified	1b RESTRICTIVE MARKINGS
2a. SECURITY CLASSIFICATION AUTHORITY unclassified	3 DISTRIBUTION / AVAILABILITY OF REPORT unlimited
2b DECLASSIFICATION / DOWNGRADING SCHEDULE	
4. PERFORMING ORGANIZATION REPORT NUMBER(S) Technical report #18	5. MONITORING ORGANIZATION REPORT NUMBER(S)
6a. NAME OF PERFORMING ORGANIZATION Hector D. Abruna Cornell University 6b. OFFICE SYMBOL (If applicable)	7a NAME OF MONITORING ORGANIZATION Office of Naval Research
6c. ADDRESS (City, State, and ZIP Code) Department of Chemistry Baker Laboratory, Cornell University Ithaca, New York 14853	7b ADDRESS (City, State, and ZIP Code) Chemistry Division 800 N. Quincy St. Arlington, VA 22217
8a. NAME OF FUNDING / SPONSORING ORGANIZATION Office of Naval Research 8b. OFFICE SYMBOL (If applicable)	9 PROCUREMENT INSTRUMENT IDENTIFICATION NUMBER N00014-84-K-0656/P00002
8c. ADDRESS (City, State, and ZIP Code) Chemistry Division 800 N. Quincy St. Arlington, VA 22217	10 SOURCE OF FUNDING NUMBERS PROGRAM ELEMENT NO. / PROJECT NO. / TASK NO. / WORK UNIT ACCESSION NO
11 TITLE (Include Security Classification) Variable Length-Scale Studies at Interfaces with X-ray Standing Waves	
12 PERSONAL AUTHOR(S) H.D. Abruna, G.M. Bommarito and D. Acevedo	
13a. TYPE OF REPORT Technical 13b. TIME COVERED FROM _____ TO _____	14. DATE OF REPORT (Year, Month, Day) 90/6/4 15. PAGE COUNT 2
16 SUPPLEMENTARY NOTATION	
17 COSATI CODES FIELD / GROUP / SUB-GROUP	18. SUBJECT TERMS (Continue on reverse if necessary and identify by block number) X-rays, synchrotron radiation, standing waves, solid/liquid interfaces.

19. ABSTRACT (Continue on reverse if necessary and identify by block number)

The principles and applications of the x-ray standing wave technique are described. Emphasis is placed on its use as a variable length-scale probe for the study of structure, composition and distribution of interfacial species especially at solid/liquid interfaces.

20 DISTRIBUTION / AVAILABILITY OF ABSTRACT ☑ UNCLASSIFIED/UNLIMITED ☐ SAME AS RPT ☐ DTIC USERS	21 ABSTRACT SECURITY CLASSIFICATION unclassified
22a NAME OF RESPONSIBLE INDIVIDUAL H. D. Abruna	22b TELEPHONE (Include Area Code) (607) 255-4720 22c. OFFICE SYMBOL

DD FORM 1473, 84 MAR 83 APR edition may be used until exhausted
All other editions are obsolete

SECURITY CLASSIFICATION OF THIS PAGE
Unclassified

Variable Length-Scale Studies at Interfaces with X-ray Standing Waves

H. D. Abruña*, G. M. Bommarito and D. Acevedo
Department of Chemistry
Baker Laboratory
Cornell University
Ithaca, New York 14853-1301

Abstract:

The principles and applications of the x-ray standing wave technique are described. Emphasis is placed on its use as a variable length-scale probe for the study of structure, composition and distribution of interfacial species especially at solid/liquid interfaces.

I. Introduction:

Structure, composition and distribution of species are key aspects that are intimately related to interfacial reactivity and their study can provide valuable insights on areas of fundamental, technological and economic relevance [1]. Particularly important are changes in the above mentioned aspects that may arise as the result of various physicochemical perturbations or stimuli such as irradiation, pH, ionic strength, electric and magnetic fields and others since in many cases reactivity will be greatly influenced. The importance of interfacial reactivity relates to a broad range of problems including among others catalysis, adsorption, electron transfer, corrosion and the potential and ionic gradients at charged interfaces including colloids, electrodes and biological membranes [2]. Many of the above mentioned areas involve the interface between a solid and a condensed phase and this has made their direct study rather elusive since most techniques sensitive to surface structure, composition and distribution can only operate under high or ultra-high vacuum.

Because of their short wavelegths and significant penetration depths, X-rays represent a unique tool with which to study structural, compositional and distributional aspects of interfacial species. The advent of powerful X-ray synchrotron sources [3] had made many of these investigations feasible and has sparked a renewed interest in such studies. Thus the development and application of techniques such as surface EXAFS [4] (Extended X-ray Absorption Fine Structure), surface diffraction [5] and X-ray standing waves [6].

In this Article we focus on the use of the X-ray standing wave (XSW) technique as a tool to probe interfacial structure, composition and distribution over a broad range of length scales. We begin with a discussion of fundamental and experimental aspects followed by a discussion of some selected examples. We finish with a view towards future applications.

X-ray standing waves arise as a result of the interference between coherently related incident a reflected plane waves [6]. Such a definition, although accurate, does little in helping one visualize the nature of standing waves and their utility in studying structural, compositional and distributional aspects of interfaces. Thus, before proceeding any further, let us consider some simple concepts that will hopefully help us understand the origin and utility of standing waves.

Consider two coherently related plane waves with the same wavelength λ. The interference of these two waves generates a standing wave (Figure 1A) with a period D given by

$$D = \lambda/2\sin\Theta \qquad (1)$$

where λ is the wavelength and 2Θ is the relative angle between the waves. If the angle of incidence is increased, the value of $2\sin\Theta$ increases and thus the period of the standing wave decreases as depicted in Figure 1B. An important property of standing waves is that the amplitude is stationary in time but a function of position. However, the standing wave can be scanned (moved) by changing the relative phase between the incident and reflected waves. Figure 1C represents the location of 3 antinodes (dashed lines) in a standing wave. By moving one wave with respect to the other one changes the relative phase between them and the net effect is a movement of the antinodes in the direction of the arrow in Figure 1D. In so doing, one is, in essence scanning the wave with respect to position.

Imagine having a species A at some fixed location where the standing wave exists. Let us assume that there is an interaction of the standing wave with this species that gives rise to a characteristic response dependent on, for example, the electric field intensity of the standing wave at the location occupied by A. Then, by monitoring the intensity of the characteristic response of A as we move the standing wave (by varying the relative phase) we can ascertain the location of A, its distribution as well as the total amount of A present. This simple description contains

all the essential elements of standing waves which we shall elaborate on below. In the interest of brevity and simplicity we shall keep the mathematical description to a minimum and concentrate on descriptive aspects as well as on the general utility of the technique.

II.Generation of Standing Waves:

As mentioned in the introduction, standing waves arise from the interference between incident and reflected plane waves. The generation of a strong standing wave requires a strong reflected wave. Within the x-ray region of the spectrum, a strong reflected wave can be generated through total external reflection or through Bragg reflection [7] and this dictates the type of standing wave generated. X-ray standing waves generated through Bragg reflection on single crystals have periods that are typical of crystallographic d-spacings; that is of the order of a few Å. The use of layered synthetic microstructres (LSMs; vide-infra) in Bragg reflection allows for the generation of XSW with d-spacings in the range of 20-200Å. Finally XSW generated through total external reflection have d-spacings in the range of hundreds of Å. Thus, by the judicious choice of experiment one can change the characteristic length-scale of the technique. A generic reflectivity profile, depicting both total external reflection and Bragg reflection, is presented in Figure 2B. We shall begin with a description of standing waves generated through Bragg reflection and then proceed on with a discussion of standing waves generated through total external reflection.

A. X-ray Standing Waves Based on Bragg Reflection:

The x-ray standing wave generated by Bragg reflection represents an extremely sensitive tool for determining the position of impurity atoms within a crystal or adsorbed onto crystal surfaces [6]. This technique is based on the XSW field

that arises as a result of the interference between the coherently related incident and Bragg diffracted beams from a perfect crystal and is described by the theory of dynamical diffraction of x-rays [8]. In the vicinity of a Bragg reflection, (Figure 2A,B) an incident plane wave (with wave vector k_O) and a reflected wave (with wave vector k_R) interfere to generate a standing wave with a periodicity equivalent to that of the (h,k,l) diffracting planes. The nodal and antinodal planes of the standing wave are parallel to the diffracting planes. The standing wave develops not only in the diffracting crystal, but also extends well beyond its surface. Estimates of this coherence length range to values as large as 1000Å from the interface [9]. As the angle of incidence is advanced through the strong Bragg reflection, the relative phase between the incident and reflected plane waves (at a fixed point) changes by π (Figure 3A). Due to this phase change, the antinodal planes of the standing wave field move towards the crystal in a direction normal to the diffraction planes by 1/2 of a d-spacing, from a position halfway between the (h,k,l) diffracting planes (or their projection) at the low angle side of the Bragg reflection to a position that coincides with them at the high angle side of the Bragg reflection (Figure 3B). Thus, the standing wave can be made to sample an adsorbate, overlayer or distributed layer at varying positions above the substrate interface. That is, XSW measurements can provide information on the concentration, position and distribution of species in the direction normal to the surface. However, it provides no in-plane information.

For an atomic overlayer which is positioned parallel to the diffracting planes, the nodal and antinodal planes of the standing wave will pass through the atom plane as the angle of incidence is advanced. By choosing the incident x-ray beam energy to be at or beyond an absorption edge for the atoms in the overlayer characteristic fluoresce can be excited. As the angle of incidence is advanced across the Bragg reflection, the fluorescence emission yield for the atoms in the overlayer will exhibit a characteristic modulation dependent on the position of the adlayer relative to the

diffraction planes. Figure 4 depicts the angular dependence of the fluorescence yield which would be observed for an adsorbate layer located at varying positions with respect to the diffracting planes. Notice the distinct differences in these profiles for positions that only differ by fractions of a d-spacing. This makes XSW measurements extremely sensitive to distributions normal to the diffraction planes.

The fluorescence emission yield can be cast in terms of an integral that incorporates an expression for the distribution function f(z) of the atoms.

$$Y(z,\Theta) = \int I(z,\Theta)\, f(z)\, dz \qquad (2)$$

The phase and amplitude of the modulation (or so-called coherent position and coherent fraction) are a measure of the mean position $\langle Z \rangle$ and width $\sqrt{\langle Z \rangle^2}$ of the distribution (f(z)) of atoms in the overlayer. Standing wave measurements of $\langle Z \rangle$ and $\sqrt{\langle Z \rangle^2}$ can be accurate to within 1% and 2% of the d-spacing, respectively [10]. The coherent fraction (f_c) and coherent position (p_c) are incorporated into the yield equation as:

$$Y(z,\Theta) = |E_o|^2 [(1+R+2\sqrt{R}\, f_c \cos(\nu - 2\pi\, p_c)] \qquad (3)$$

where E_o is the incident electric field amplitude, R is the reflectivity and ν is the phase. The coherent fraction (f_c) reflects the distribution of atoms in the adlayer. For example if all the atoms were at the same position (i.e. a distribution described by a delta function) the coherent fraction would be one. On the other hand, if the atoms were randomly distributed (normal to the surface) the coherent fraction would be zero. For intermediate cases the coherent fraction would have a value between zero and one. When the atoms are distributed over a range of distances, the coherent fraction represents the integral of the function describing such a distribution. Most often, the distribution is assumed to be gaussian in shape.

Since the Z scale of the Bragg reflection XSW is modulo-d (that is positions are obtained with respect to the diffraction planes so that the Z scale is not absolute), if several coherent positions (in Z) are possible for the adsorbate, a single measurement will not be sufficient to unambiguously determine these positions. Thus, XSW measurements with a different period (such as higher order Bragg reflection measurements or total external reflection) must be performed to allow such an assignment.

One of the problems associated with the implementation of the standing wave technique based on Bragg reflection is the fact that it requires the use of perfect or nearly perfect crystals. Thus, most experiments have been performed on silicon or germanium single crystals [11,12]. In addition, although the characteristic modulo-d length scale of a few angstroms of XSW generated by Bragg reflection from single crystals is ideal for determining bond lengths between atom layers at single crystal surfaces, it is inappropriate for the structural determination of systems extending over several tens of angstroms (e.g. ionic distributions at charged surfaces).

An alternative to single crystals is the use of synthetic layered microstructures (LSM)[13] which are depth-periodic structures consisting of alternating layers of high and low electron density materials (such as tungsten and silicon, or platinum and carbon), and which are of high enough quality to produce strong Bragg reflection (Figure 2A,C). In essence, the combination of high and low electron density layers mimics the electron density patterns in single crystals. LSMs are advantageous for XSW studies because they can be made with fundamental d-spacings ranging from 20 to 200Å and these give rise to long period XSW standing waves which are optimally suited to investigate systems that are distributed over such distances. LSMs can be prepared from a wide range of materials and the experimenter can choose the material to be used as the multilayer's top surface. Experimental reflection curves from LSMs compare well with predictions from dynamical

diffraction theory with peak reflectivities as high as 80%. Therefore, a well defined standing wave can be produced. LSMs also possess surfaces of mirror quality, making them excellent x-ray reflectors so that they can also be used as substrates for generating total external or specular reflection XSWs. Furthermore, LSMs have Bragg reflection angular widths of the order of milliradians which considerably simplifies experimental design.

In our work we have made extensive use of Pt/C LSMs and some of our results will be described in a later section.

B. X-ray Standing Waves Generated by Total External Reflection:

A second way of generating an XSW is through total external reflection [14]. This is based on the fact that at x-ray energies the index of refraction of matter is slightly less than one [7,15]. The critical angle for total reflection is given by:

$$\theta_{crit} = \sqrt{2\delta} \qquad (4)$$

At a given wavelength, δ depends only on the properties of the mirror material and is of the order of 10^{-6}. Θ_{crit} is typically a few milliradians. (For example, the critical angle for gold for 10keV x-rays is about 8 mrad.) As long as the x-ray beam is incident below this critical angle only an exponentially damped evanescent wave penetrates into the medium. In addition, the incident and specularly reflected plane waves interfere to form a standing wave in the more optically dense medium above the mirror surface. Thus, once again we have incident and reflected plane waves generating an XSW. Analogous to XSW generation via Bragg diffraction, there is a change in the relative phase (by π) between the incident and reflected waves and the change occurs as we scan across the critical angle. The angular dependence of the total external reflection XSW can be described using the general formalism described previously. When the angle of incidence is zero, there is a node at the mirror

surface (the incident and reflected waves are completely out of phase) and since the period D is infinite ($D=\infty$ since $\sin(0) = 0$; Equation 1) the first antinode is at infinity. As the angle of incidence is increased, the first antinode moves inward, in a direction normal to the surface, until at the critical angle it coincides with the mirror surface. The subsequent antinodes follow behind with a periodic spacing given by Equation 1. Thus, the angular variation of the total external reflection XSW can be visualized as a wave that is compressing and shifting downwards towards the surface as the angle of incidence is advanced (i.e., both the period and the pahse are changing simultaneously) .

For XSW generated through TER, one can define a critical period D_{crit} which is that when $\Theta = \Theta_{crit}$. Since the reflectivity drops precipitously beyond the critical angle (Figure 2B), there is a limited range of angles (and thus D spacings) over which a strong standing wave can be generated. For example, for a 10keV photon the critical angle for gold is about 7.8 mrad. (recall that 1 degree is about 17.5 mrad.) so that the critical period is about 80Å. On the other hand, the critical period for silicon under similar conditions is about 200Å. Thus, under conditions of total external reflection, very large period XSW are generated and these are useful in the investigation of distributions that extend over these very large distances.

III. Experimental Aspects and Data Analysis:

XSW experiments are generally, rather demanding and alignment of the sample relative to the beam is critical. An XSW experiment consists of monitoring the angular dependence of some signal arising from the species of interest and which is proportional to the standing wave electric field intensity (such as characteristic fluorescence). A typical experimental set up is shown in Figure 5. Of particular importance is the angular resolution of the sample stage since the typical reflection width for a single crystal will be of the order of tens of microradians and a few

milliradians for LSMs. In addition, when measuring fluorescence from an adsorbate layer, care must be taken to accurately subtract background radiation.

Analysis of x-ray standing wave data is based on a fit of the data (reflectivity and fluorescence yield) to predictions from theory. However, the data must first be treated to extract yields corrected for background and other contributions. In general, the fluorescence yield is recorded as a function of angle of incidence and an x-ray fluorescence spectrum is also acquired at each angular position. Fitting of the desired characteristic fluorescence emission line to an assumed functional form (usually a combination of Gaussian functions) and subtraction of an extrapolated polynomial background render the data suitable for reconstruction of the fluorescence yield as a function of the angle of the incident radiation.

In order to fit the data, the electric field intensity at a particular point must either be calculated form dynamical diffraction theory [8] or from an optical theory approach. The latter is based on a stratified medium formalism in which the medium is divided into parallel slabs [13a,16]. The continuity of the tangential components of the electric and magnetic fields at each of the resulting interfaces is the essential requirement to obtain a recursion relation (containing Fresnel coefficients) describing the electric field amplitudes at each interface for the incident reflected and refracted waves. Such a treatment is applicable to the total external reflection condition as well as to Bragg diffraction. The layered medium approach is particularly well suited for analysis of standing waves in multilayered structures [13a,17].

Incorporation of coherent position and coherent fraction into equation 3 (or analogous expressions) allows a fit to be obtained in terms of three parameters: normalized coverage of absorber, coherent position, and coherent fraction.

IV.Selected Examples:

The use of XSW generated by Bragg reflection on perfect single crystals (such as Si and Ge) has been employed in numerous studies of adsorbates on surfaces. In fact these studies represent a large fraction of the XSW measurements carried out to date. As mentioned before, the first observation of an XSW based on Bragg reflection was by Batterman [6] who monitored the Ge_K fluorescence from a perfect Ge single crystal as the angle was scanned across the (220) reflection.

Golovchenko and coworkers [11] were the first employ this technique to study adsorbates by monitoring the angular dependence of the fluorescence yield of bromine chemisorbed onto a Si(111) crystal. In this study experiments were performed while the crystal was covered by a thin film of methanol pointing to the feasibility of performing experiments at the solid/liquid interface. The technique has since been employed in numerous other studies [18].

As electrochemists, our interest lies in the use of the XSW technique to study solid/liquid interfaces, in general, and the electrode solution interface in particular. We are especially interested in being able to follow potential dependent variations in the distribution of species in the vicinity of the electrode surface. Such variations are a strong function of the applied potential and can cover distances as small as few and as large as hundreds of Ångstroms. Furthermore, the use of x-rays as probes allows for the in-situ characterization of such systems. Thus, the ability to use an in-situ probe whose characteristic length scale can be varied over such a broad range, makes XSW ideal for the study of solid/liquid interfaces in general.

In our studies, the substrate material on which the reflected wave is generated also serves as the electrode whose potential we wish to change over a broad range. As a result, in our work we have relied heavily on Pt/C LSMs as substrates since they fulfill all of our requirements in addition to providing all of the advantages previously mentioned.

We shall discuss four different examples which cover a variety of length scales and experimental situations and these are:

1. Electrodeposition of Copper on an Iodine Treated Pt/C LSM
2. Packing Density and Potential Dependent Distributional Changes of Iodine on a Pt/C LSM
3. XSW Study of a Redox Active Self-Assembling Monolayer
4. Long Period XSW Study of Ionic Distributions at a Surface Immobilized Phospholipid Membrane

The first example deals with distributions that occur over a very short range (<5Å). In the second, we discuss potential dependent distributions that extend over hundreds of Å's whereas the third example involves measurements in the range of 20Å's. Finally, and for completion, we present an example on the use of XSW generated by total external reflection to study ionic distributions at phospholipid monolayers.

1. Electrodeposition of Copper on an Iodine Treated Pt/C LSM

One of our earlier XSW studies involved the adsorption of iodide onto a platinum/carbon LSM followed by the electrodeposition of a layer of copper [19]. The LSM sample consisted of 15 platinum/carbon layer pairs with each layer having 26 and 30 Å of platinum and carbon, respectively, with platinum as the outermost layer. 9.2 keV radiation from the Cornell High Energy Synchrotron Source (CHESS) was used to excite L-level and K-level fluorescence from the iodide and copper, respectively. Initially, the LSM was contacted with a 35 mM aqueous solution of sodium iodide for 15 minutes. It was then studied by the x-ray standing wave technique. The characteristic iodine L fluorescence could be detected and its angular dependence was indicative of the fact that the iodine layer was on top of the platinum surface layer. A well-developed reflectivity curve (collected simultaneously) was also

obtained. Following this, the LSM was placed in an electrochemical cell and half a monolayer of copper was electrodeposited. The LSM (now with half a monolayer of copper and monolayer of iodide) was again analyzed by the x-ray standing wave technique. Since the incident x-ray energy (9.2 keV) was capable of exciting fluorescence from both the copper and iodide, the fluorescence intensity of both elements (as well as the reflectivity) were obtained simultaneously. The results presented in Figure 6 show the reflectivity curve and the modulations of the iodide and copper fluorescence intensities. The most important feature is the noticeable phase difference between the iodide and copper modulation, i.e. the location of the iodide and copper fluorescence maxima, with the copper maximum being to the right of the iodine maximum. Since the antinodes of the XSW move inward as the angle increases, the order in which these maxima occur can be unambiguously interpreted as meaning that the copper layer is closer than the iodide layer to the surface of the platinum. Since the iodide had been previously deposited on the platinum this represents unequivocal evidence of the displacement of the iodide layer by the electrodeposited copper. Similar findings based on Auger intensities and LEED patterns have been previously reported by Hubbard and co-workers [20].

From an analysis of the copper fluorescence intensity we were able to determine that the copper layer had a significant degree of coherence (f_C =0.53) and that its coherent position was 0.70Å above the platinum surface. Similar analysis of the iodine fluorescence gave values of 0.40 and 4Å for the coherent fraction and position, respectively. Although we were not aware of it at that time, the distances obtained from this measurement also shed some light on the nature of bonding within the deposited layer. From the values of the coherent positions, we can extract a Cu-I bond distance and this is closer to that for CuI than for a metallic copper layer in contact with an iodine layer suggesting that, as deposited, there is a significant degree of partial charge transfer from copper to iodine. We have recently arrived at

the same conclusions based on voltammetric and x-ray absorption spectroscopic measurements on the same system [21].

This case exemplifies the study of systems whose distribution extends over a very short range close to the electrode surface.

2. Iodine on Pt: Packing Density and Potential Dependent Distributional Changes:

The adsorption of iodide on polycrystalline and single crystal Pt electrodes has been widely investigated using LEED, Auger, EXAFS and voltammetric techniques. It is generally accepted that immersion of a Pt(111) surface into aqueous iodide (or HI) solutions results in the formation of an ordered ad-layer of iodine atoms. Furthermore, the Pt(111)/I system possesses a rich potential-dependent coverage isotherm, which has been characterized by Auger spectroscopy for the emersed case [22], and in-situ by x-ray absorption spectroscopy [23]. Its features are explained in terms of potential dependent structural and distributional changes. The aim in this work was to study in-situ, via the XSW method using LSMs, the potential dependence of structural changes in the distribution of iodine species, and to relate features of the aforementioned isotherm to observations from this measurement [24]. In this measurement we employed a 40.8 Å d-spacing Pt/C LSM (Pt as the top-most layer) in contact with a 0.1M Na_2SO_4 solution of pH 6.7 containing 10μM NaI.

As mentioned in a previous section, coherent position and coherent fraction can be used to describe the distribution of species determined from XSW measurements. However, these terms are relevant only when describing symmetrical atomic distributions centered around a given mean (<Z>) position. For an extended (i.e. a distribution with width >d), unsymmetrical distribution N(z), coherent position and coherent fraction are inadequate in characterizing the angular dependence of the XSW fluorescence yield . In this case, a model for N(z) must be

chosen and the standing wave electric-field intensity $I(\Theta,z)$ must be averaged over the entire distribution:

$$Y(\Theta) = \int I(\Theta,z)\, N(z)\, dz \qquad (5)$$

In this study, we chose the simple model depicted in Fig. 7A to describe the iodide distribution. The model consists of three basic components: (1) a step at the electrode's surface extending over a few Angstroms, describing the specifically adsorbed iodine atoms, (2) an exponential tail with a characteristic decay length k, extending out into solution from the iodine ad-layer, portraying iodide anions attracted to the electrode surface (the diffuse layer), and (3) a second step, with a width equal to the thickness of the solution layer, depicting bulk iodide. Analytically, this model can be expressed as follows:

$$N(z) = \begin{cases} N_{ad} & 0 \le z \le t_{ad} \\ N_{diff} \exp(-z/k) & t_{ad} < z \le t_{sol} \end{cases} \qquad (6)$$

where: N_{ad} is the concentration of iodine atoms specifically adsorbed, t_{ad} is the ad-layer thickness, N_{diff} is the initial concentration of iodide in the diffuse layer, k is the decay length of this diffuse layer, N_{bulk} is the iodide bulk concentration, and t_{sol} is the thickness of the solution layer. The choice of an exponential decay to model the diffuse layer was motivated by its mathematical simplicity as well as its frequent usage in simple theoretical descriptions of the electrical double layer [25]. The standing wave yield can now be calculated using the distribution N(z) defined above (Equation 5) in the integral in Equation 4. Computationally, N_{diff} and N_{bulk} were expressed as fractional values of N_{ad} and the distribution was normalized using the condition:

$$Y_{OB} = \int_{Z=0}^{t_{sol}} N(z)\, dz \qquad (7)$$

where Y_{OB} is the measured off-Bragg fluorescence yield; a value proportional to the total number of I/I^- species present in the solution layer (t_{sol}). As a result, the model has three free parameters: the ad-layer thickness t_{ad}, the fractional quantity N_{diff}/N_{ad}, and the decay length k. The remaining parameters are held constant; the ratio N_{bulk}/N_{ad} is known, and the thickness t_{sol} can be determined experimentally using the measured x-ray reflectivity.

The effect of including a diffuse layer along with the adsorbed layer in the model (Equation 6), corresponds to a superposition of a random-like component to the coherent XSW yield from the ad-layer (provided that the thickness t_{ad} is narrow with respect to the substrate's d-spacing), in a ratio proportional to the population in each layer with the number of atoms in the diffuse layer being controlled by the decay length k and the initial concentration N_{diff}. From theoretical calculations, we find that the XSW technique is very sensitive to these distributional changes. For example, adding a diffuse layer with a fall-off length of only 10 Å produces a dramatic change in both the amplitude and the phase of the calculated signal. Furthermore, appreciable differences are seen when the diffuse layer population is changed by varying N_{diff}. Thus, in principle, the XSW method is extremely sensitive to subtle changes in atomic/ionic distributions at the electrode/electrolyte interface.

The I_L fluorescence yield as a function of the angle of incidence Θ, for each of the potentials studied, is shown in Fig. 8. As we discussed previously, changes in both the phase and amplitude of the standing wave signal are indicative of distributional changes in the direction normal to the substrate surface. In addition, the potential dependent changes in the background slope, peak position, and modulation amplitude, provide further insights as to the distribution of species. All of the variations in these parameters can be understood in terms of changes in the distribution of iodine/iodide species at the electrode/electrolyte interface as

described by the above mentioned model where each of the three components makes a distinct contribution to the overall standing wave fluorescence yield.

In order to obtain a quantitative assessment of the contribution of the various components, we have χ^2 fitted the data to theoretical yields based on the model defined in Equation 6. Figure 9 shows two typical theoretical fits, and points out the noticeable differences produced in the fluorescence yield by two different iodide distributions. Referring to this figure, if the diffuse layer had been a negligible component of the iodide distribution, the observed fluorescence yield would have followed the theoretical yield calculated for an ad-layer alone (blue lines). On the other hand, if the bulk or diffuse layer contributions were dominant the fluorescence yield would have been that calculated for a random distribution (magenta lines). In both cases the best fit represents a combination of these two limiting cases.

The changes in ad-layer normalized coverage with applied potential are presented in Figure 7. These values were obtained by taking the off-Bragg yield at each potential and subtracting the contribution due to the diffuse layer, as determined from the fitting parameters k and N_{diff}/N_{ad}. The variations in the normalized coverage are analogous to packing densities observed on Pt(111) from dilute NaI solution by in-situ x-ray absorption spectroscopy [23] and on emersed Pt(111) by Auger electron spectroscopy [22]. In these cases, these changes are attributed to structural changes in the adsorbed iodine ad-layer.

Since the changes observed in the normalized coverage in this experiment are in excellent agreement with the changes in the packing density measured on a Pt(111) electrode surface we believe that a similar structural transition takes place for the iodine ad-layer formed at the Pt surface of the Pt/C LSM employed in this work.

In view of the conclusions drawn from analysis of the standing wave and off-Bragg yield measurements, we depict the potential dependent I/I^- distributional changes in Figure 7B. From this quantitative picture, we note a marked accumulation of iodide in the diffuse layer, weakly associated with the adsorbed iodine, when the Pt surface is not saturated by iodine adatoms (-0.1V). Perhaps, this striking association of iodide with the iodine ad-lattice is driven by the hydrophilic character of the unsaturated Pt surface. Furthermore, the increase in the adsorbed iodine packing density to saturation coverage is accompanied by an abrupt decrease in the concentration of this accumulated iodide. Thus, we suggest that the potential dependent structural transformation in the iodine ad-lattice could be viewed as a phase transition, in which iodide anions in the liquid-like arrangement of the diffuse layer are incorporated into the crystalline-like structure of the iodine ad-lattice, resulting in a saturated Pt surface, possibly hydrophobic, and the concomitant decrease in the concentration of iodide in the diffuse layer, associated with the adsorbed iodine.

In this work, we were able to follow, in-situ, distributional changes for a minute amount of an ionic content, with Ångstroms resolution in the direction normal to the surface. The model chosen to describe this distribution was primitive; more complex models, using liquid-pair distribution functions, might describe the diffuse layer more rigorously. However, to discern unambiguously the value of each of the many parameters used to define these types of distributions, a collection of standing wave measurements, over higher order Bragg reflections as well as the total external reflection regime, must be available for analysis. In this regard, we are carrying out standing wave experiments, of this and similar systems, in the total external reflection region.

3. XSW Study of a Redox Active Self-Assembling Monolayer

Because of their relevance to a multitude of problems of fundamental, technological and economic importance, the study of reactions within organized media, both in solution as well as at interfaces, has received a great deal of attention in the recent past [26]. Within the present context, it is reactions taking place at interfaces of controlled and deliberate architecture that are of interest and specifically those which involve redox active components. Various techniques have been employed in the preparation of such structured interfaces with those based on the Langmuir-Blodgett and self-assembly techniques having received the most attention. The potential applications of structured interfaces are numerous and include imaging, sensing, diagnostics and many others.

The study of electron transfer kinetics for surface immobilized redox species has received a great deal of attention especially with regards to the distance dependence of the rate since it is believed that they may provide very valuable insights on long-range electron transfer processes within biological systems [27]. Because they are structurally simpler (and ostensibly better characterized), these model studies may allow for a clearer and more direct interpretation. However, most such studies have been plagued by the difficulty of being able to measure directly the distance between the redox active center and the electrode surface. As a result, the distance is often inferred from indirect measurements. Unfortunately, such estimates can lead to serious errors due to the extreme sensitivity of the rate of electron transfer on distance (estimated to be about one order of magnitude per Å change in distance).

We describe here some preliminary results of an XSW study of a redox active self-assembling monolayer [28] and point to some of the advantages and difficulties of such measurements.

The system studied was the osmium complex $[Os(bpy)_2(dpyp)Cl]^{1+}$ (bpy is 2,2' bipyridine and dpyp is 1,3-di-(4-pyridil) propane) whose structure is presented in Figure 10A. This material was specifically prepared for these studies since it fulfills all of the necessary requirements. First of all, the remote pyridine group provides a site of attachment to an electrode surface. The complex exhibits reversible electrochemistry and is stable in both oxidized and reduced forms. An added bonus was the fact that the redox transformation occurs at a very convenient potential ($E^{\circ\prime}$ = +0.25 and +.130 V vs SSCE in methylene chloride and water, respectively). In addition the osmium L fluorescence at 8.9 keV is in a very convenient region of the spectrum.

This material adsorbs very strongly to platinum electrodes and the surface immobilized complex exhibits very well behaved electrochemistry (Figure 10B) in numerous solvents. A saturation coverage representing a compact monolayer (1 monolayer represents $1x10^{-10}$ mol/cm^2) is achieved for solution concentrations above 4μM. A typical adsorption isotherm is presented in Figure 10C. Thus, this system appeared very well suited to investigations by XSW.

In this experiment we employed a 40.8Å d-spacing Pt/C LSM as the electrode. A monolayer of complex was adsorbed from solution and the electrode was mounted in an electrochemical cell similar to that used in previous studies. An incident x-ray beam energy of 11.1keV was employed to excite Os_L fluorescence. In all cases a reflectivity profile was collected simultaneously with the Os_L fluorescence intensity. Experiments were carried out at applied potentials of 0.0 and +0.50 V where the osmium center within the complex is present as Os(II) and Os(III), respectively. It should be noted that the overall charge on the complex changes from +1 to +2 upon electrochemical oxidation.

Data for the Os_L fluorescence intensity at 0.0 and +0.50 V as well as a reflectivity profile are presented in Figure 10D. Again, as in the previous examples

we focus on the angular position of the fluorescence maxima and on the width of the fluorescence profile. As can be seen in Figure 10D, the maximum in the fluorescence at 0.0 V occurs at a lower angle than at +0.50. In addition, the fluorescence intensity is lower and the distribution broader at +0.50 V relative to the values at 0.0 V. There are some qualitative observations that may be made. The fact that upon oxidation at 0.50 V the fluorescence maximum shifts to a higher angle suggests that, on average, the osmium centers are closer to the electrode surface than at 0.0 V. It is worth mentioning that the distance between the osmium center and the electrode surface would be 12 Å for a fully extended chain.

The fact that the fluorescence yield profile is wider at +0.50 relative to 0.0 V would suggest that there is a broader distribution of distances. This might be due to increased coulombic repulsion between adjacent molecules since upon oxidation the charge on each molecule increases from +1 to +2. Thus, the coulombic repulsion is expected to be approximately four times as large and in order to release the repulsive forces, the molecules may adopt a broader distribution in terms of distance. Although these are preliminary findings, our interpretation is consistent with the data. In addition, additional electrochemical evidence is also consistent with the interpretation given above.

We are now preparing analogous molecules with varying chain length between the pyridines in order to carry out a systematic study of potential dependent variations as a function of chain length. We feel confident that these studies will provide a wealth of information on electron transfer rates and reactivity of redox monolayers on electrodes.

4. Study of Ionic Distributions at a Surface Immobilized Phospholipid Membrane Using Total External Reflection XSW.

In the interest of completeness, we briefly describe a recently reported XSW study on ionic distributions at a phospholipid membrane [29]. There is much interest in the study of such systems because of the importance of membrane potentials in numerous biological processes as well as on the resulting ionic gradients.

These investigators employed a 27Å thick phospholipid membrane deposited by the Langmuir-Blodgett method onto a 35Å d-spacing Si/W LSM (Si as the outermost surface) which had been previously coated with a layer of dimethylsilane in order to render the surface hydrophobic. In order to enhance stability, the phospholipid membrane was photopolymerized. Although the LSM could have been used to generate an XSW based on Bragg reflection, this study employed an XSW generated through total external reflection.

The purpose of this study was to follow the distribution of ionic species (Zn^{+2}) in the vicinity of the phosphate head group by varying the surface potential which was achieved by varying the pH of the contacting medium. At low pH values the phosphate group would be largely protonated so that there would be no net charge on the membrane. Under these conditions the surface potential would be close to zero and as a result there would be very little (if any) electrostatic attraction of the Zn^{+2} ions. Thus the distribution of Zn^{+2} ions in the vicinity of the membrane would be expected to be random. Conversely, at high pH the phosphate groups would be ionized and the resulting negative charge would strongly attract the Zn^{+2} ions towards the membrane surface. At intermediate pH values a combination of these two limiting cases would be expected. Experiments were carried out at pH values of 2.0, 4.4 and 6.8.

The results can be summarized as follows:

(1) The surface concentration of Zn^{+2} is the same at pH=6.8 and 4.4 (.31M) but drops to almost 1/2 at pH=2.0 (.18M). This indicates a lack of competition for condensation on the monolayer between the Zn^{+2} ions and the protons present in solution for the higher pHs. The drop in Zn^{+2} surface concentration at pH=2.0 is evidence of this competition with protons for condensation on the phospholipid membrane.

(2) The changes in surface concentrations of Zn^{+2} and H^{+} ions are responsible for dramatic changes of the surface charge, which in turn alters drastically the extent of the diffuse part of the double layer. This is illustrated by the observed 1/k values at the different pHs (Figure 11). At pH=6.8 1/k=56Å whereas for the two lower pH values 1/k is approximately 5Å. These observations imply that the surface charge at the higher pH is actually less negative than for pH=4.4 and 2.0, in other words, addition of an excess of the monovalent ion charges the phospholipid membrane.

A comparison of the concentration profiles obtained from the XSW experiment and those calculated from Gouy-Chapman theory show good agreement.

V. Future prospects and applications:

It is clear that the XSW technique is a powerful probe of the structure, composition and distribution of interfacial species and is of particular value in the study of solid/liquid interfaces. The fact that the length-scale that it probes can be controlled is an especially attractive feature. In addition, the construction of new synchrotron radiation facilities will also make this technique accessible to a broader range of practitioners. As more emphasis if placed on the investigation of interfacial properties of biological systems and new materials, we feel confident that the XSW technique will play an increasingly prominent role in these investigations.

Acknowledgements:

This work was generously supported by the Materials Chemistry Initiative of the National Science Foundation, the Office of Naval Research, the Materials Science Center at Cornell University, the Army Research Office, Eastman Kodak Co., Dow Chemical Co. and Xerox Corp. HDA is a recipient of a Presidential Young Investigator Award and a Sloan Foundation Fellowship. DA acknowledges support by a MARC Fellowship of the National Institutes of Health.

The help of J.H. White, M.J. Bedzyk, M. McMillan, J. F. Rodríguez and the CHESS staff is greatly appreciated. The work described here was performed at the Cornell High Energy Synchrotron Source (CHESS) which is supported by the National Science Foundation.

Literature Cited

1. a. G. A. Somorjai, *Chemistry in Two Dimensions: Surfaces*; Cornell University Press, London, 1981.
   b. A. W. Adamson, *Physical Chemistry of Surfaces*, 4th Ed.; Wiley, New York, 1982.
2. J. N. Israelachvili, *Intermolecular an Surface Forces*, Academic Press, London, 1985.
3. H. Winick, S. Doniach, eds. *"Synchrotron Radiation Research"*, Plenum, New York, 1980.
4. a. P. H. Citrin, *Jnl. de Phys. Coll. C8* **47**, 437 (1986).
   b. B. K. Teo, *Accts. Chem. Res.* **13**, 412 (1980).
   c. P. A. Lee, P. H. Citrin, P. Eisenberger, B. M. Kincaid, *Rev. Mod. Phys.* **53**, 769 (1981).
   d. B. K. Teo, D. C. Joy, eds. *"EXAFS Spectroscopy; Techniques and Applications"*, Plenum, New York, 1981.
5. a. W. C. Marra, P. Eisenberger, A. Y. Cho, *J. Appl. Phys.* **50**, 6927 (1979).
   b. P. Eisenberger and W. C. Marra, *Phys. Rev. Lett.* **46**, 1081 (1981).
   c. I. K. Robinson, *Phys. Rev. B*, **33**, 3830 (1986).
   d. I. K. Robinson, In *Handbook on Synchrotron Radiation*, D. Moncton and G.S. Brown, ed., North Holland, Amsterdam, 1988.
6. B. W. Batterman, *Phys. Rev.* **133**, A759 (1964).
7. R. W. James, *The Optical Principles of the Diffraction of X-rays*, Oxbow Press, Woodbridge, Connecticut, 1982.
8. M. von Laue, *Roentgenstrahlinterenzen* (Akademische Verlargsgesellshaft, Frankfurt, 1960). For a review, see B. W. Batterman and H. Cole, *Rev. Mod. Phys.* **36**, 681 (1964).
9. T. W. Barbee and J. H. Underwood, *Optics Comm.* **48**, 161 (1983).
10. M. J. Bedzyk and G. Materlik, *Phys. Rev. B*, **31**, 4110 (1985).
11. P. L. Cowan, J. A. Golovchenko, M. F. Robbins, *Phys. Rev. Lett.* **44**, 1680 (1980).
12. M. J. Bedzyk and G. Materlik, *Phys. Rev. B*, **31**, 4110 (1985).

13. a. J. H. Underwood, T. W. Barbee, In *AIP Conf. Proc.* **75**, 170, D.T. Atwood, B.L. Henke, eds., AIP, New York, 1981.

b. B. Vidal and P. Vincent, *Applied Optics*, **23**,1794 (1984).

c. T. W. Barbee, *Superlattices and Microstructures*, **1**, 311 (1985).

d. D. B. McWhan, In *Synthetic Modulated Structures*, L. L. Chang, B. C. Giessen, eds., Academic Press, New York, p. 43, 1985.

14. a. M. J. Bedzyk, D. H. Bilderback, G. M. Bommarito, M. Caffrey, J. S. Schildkraut, *Science*, **241**, 1788 (1988).

b. M. J. Bedzyk, G. M. Bommarito, J. S. Schildkraut, *Phys. Rev. Lett.* **62**, 1376 (1989).

15. The index of refraction of matter is slightly less than one and is given by:

$$n = 1 - \delta - i\beta$$

$$\delta = \frac{1}{2\pi}\left(\frac{e^2}{mc^2}\right)\left(\frac{N_o\rho}{A}\right)[z + \Delta f']\lambda^2$$

$$\beta = \frac{\lambda\mu}{4\pi}$$

where $(e^2/(mc^2)$ is the classical electron radius, $(N_O\rho/A)$ is the number of atoms per unit volume, N_O is Avogadro's number, ρ is the density, A is the atomic weight, z is the atomic number, and λ is the wavelength of the x-ray. The term $[z + \Delta f']$ is the real part of the scattering factor (including the so-called dispersion term f') and is essentially equal to Z. The imaginary part of the index of refraction β is related to absorption, where μ is the linear absorption coefficient.

16. L. G. Parratt, *Phys. Rev.* **95**, 359 (1954).

17. G. M. Bommarito, M.S. Thesis, Cornell University, 1987.

18. Some representative studies include:

a. J. A. Golovchenko, J. R. Patel, D. R. Kaplan, P. L. Cowan, M. J. Bedzyk, *Phys. Rev. Lett.* **49**, 560 (1982).

b. G. Materlik, M. Schmah, J. Zegenhagen, W. Uelhoff, *Ber. Bunsenges. Phys. Chem.* **91**, 292 (1987).

c. L. E. Berman, B. W. Batterman, J. M. Blakely, *Phys. Rev. B*, **38**, 5397 (1988).

d. J. Zegenhagen, K.-G. Huang, W. M. Gibson, B. D. Hunt, L. J. Schowalter, *Phys. Rev. B*, **39**, 10254 (1989).

19. M. J. Bedzyk, D. Bilderback, J. H. White, H. D. Abruña, G. M. Bommarito, J. *Phys. Chem.* **90**, 4926 (1986).

20. a. J. L. Stickney, S. D. Rosasco, A. T. Hubbard, *J. Electrochem. Soc.* **131**, 260 (1984).

b. J. L. Stickney, S. D. Rosasco, B. C. Schardt, A. T. Hubbard, *J. Phys. Chem.* **88**, 251 (1984).

21. J. H. White and H. D. Abruña, *J. Phys. Chem.* **94**, 894 (1990).

22. F. Lu, G. N. Salaita, H. Baltruschat, A. T. Hubbard, *J. Electroanal. Chem.* **222**, 305 (1987).

23. J. H. White and H.D. Abruña, *J. Phys. Chem.* **92**, 7131 (1988).

24. G. M. Bommarito, J. H. White, H. D. Abruña, *J. Phys. Chem.* (accepted)

24. P. Delahay, *"Double Layer and Electrode Kinetics"*, Wiley-Interscience, New York, 1965.

25. a. J. H. Fendler, *Membrane Mimetic Chemistry*, Wiley-Interscience, New York 1982.

b. J. D. Swallen, D. L. Allara, J. D. Andrade, E. A. Chandross, S. Garoff, J. Israelachvili, T. J. McCarthy, R. Murray, R. F. Pease, J. F. Rabolt, K. J. Wynne, H. Yu, *Langmuir*, **3**, 932 (1987).

26. H. Kuhn, *Pure & Appl. Chem.* **51**, 341 (1979).

27. D. Acevedo and H. D. Abruña (manuscript in preparation).

28. M. J. Bedzyk, G. M. Bommarito, M. Caffrey, T. L. Penner, *Science*, **248**, 52 (1990).

Figure Legends:

Figure 1. A. Depiction of the interference between two plane waves to generate a standing wave.

B. Depiction of the change (decrease) in the standing wave period as the angle of incidence is increased relative to that in A.

C and D. Depiction of the movement of a standing wave with respect to position by changing the relative phase between the interfering waves.

Figure 2. A. Depiction of the generation of an X-ray standing wave by Bragg reflection from a Pt/C layered synthetic microstructure. k_o and k_R refer to the wave vectors of incident and reflected plane waves, respectively and Q is the momentum transfer.

B. Generic reflectivity profile depicting total external (specular) and Bragg reflection.

C. Diagrammatic depiction of an LSM.

Figure 3 A. Angular dependence across a Bragg reflection of the reflectivity and relative phase.

B. Depiction of the movement of the electric field intensity of a standing wave as the angle of incidence is scanned from the low to the high angle side of a Bragg reflection.

Figure 4. Angular dependence of the reflectivity and the the fluorescence yield (or electric filed intensity) for an atomic layer located at various positions with respect to the diffraction planes.

Figure 5. Experimental setup for an XSW experiment.

Figure 6. Reflectivity profile and normalized fluorescence yields for I and Cu for a Pt/C LSM with an electrodeposited layer of copper and adsorbed iodide. Inset: Depiction of the location of the I and Cu layers on the Pt/C LSM.

Figure 7. A. Schematic depiction of the model used to describe the distribution of iodide at a platinum surface.

B. Illustration of the changes in the iodine/iodide distribution as a function of applied potential.

Figure 8. A. Angular dependence of the I_L fluorescence intensity as a function of applied potential.

B. Reflectivity profile.

Figure 9. Theoretical fits (red lines) of I_L fluorescence intensity obtained at +0.3 (a) and -0.1 (b) V. Also shown on both panels are the theoretical yields predicted for a 10Å iodine ad-layer alone (blue lines) as well as for a random distribution of iodide in solution (magenta lines).

Figure 10. A. Structure of self-assembling, redox active osmium complex.

B. Cyclic voltammetric response in dichloromethane for the osmium complex adsorbed on a platinum electrode.

C. Isotherm for the adsorption of the osmium complex onto a platinum electrode surface.

D. Reflectivity profile and angular dependence of the Os_L fluorescence intensity at 0.00 and +0.50 V for a Pt/C LSM coated with a monolayer of the osmium complex.

Figure 11. pH dependence of the Zn^{+2} ionic distribution profiles at a phospholipid membrane.

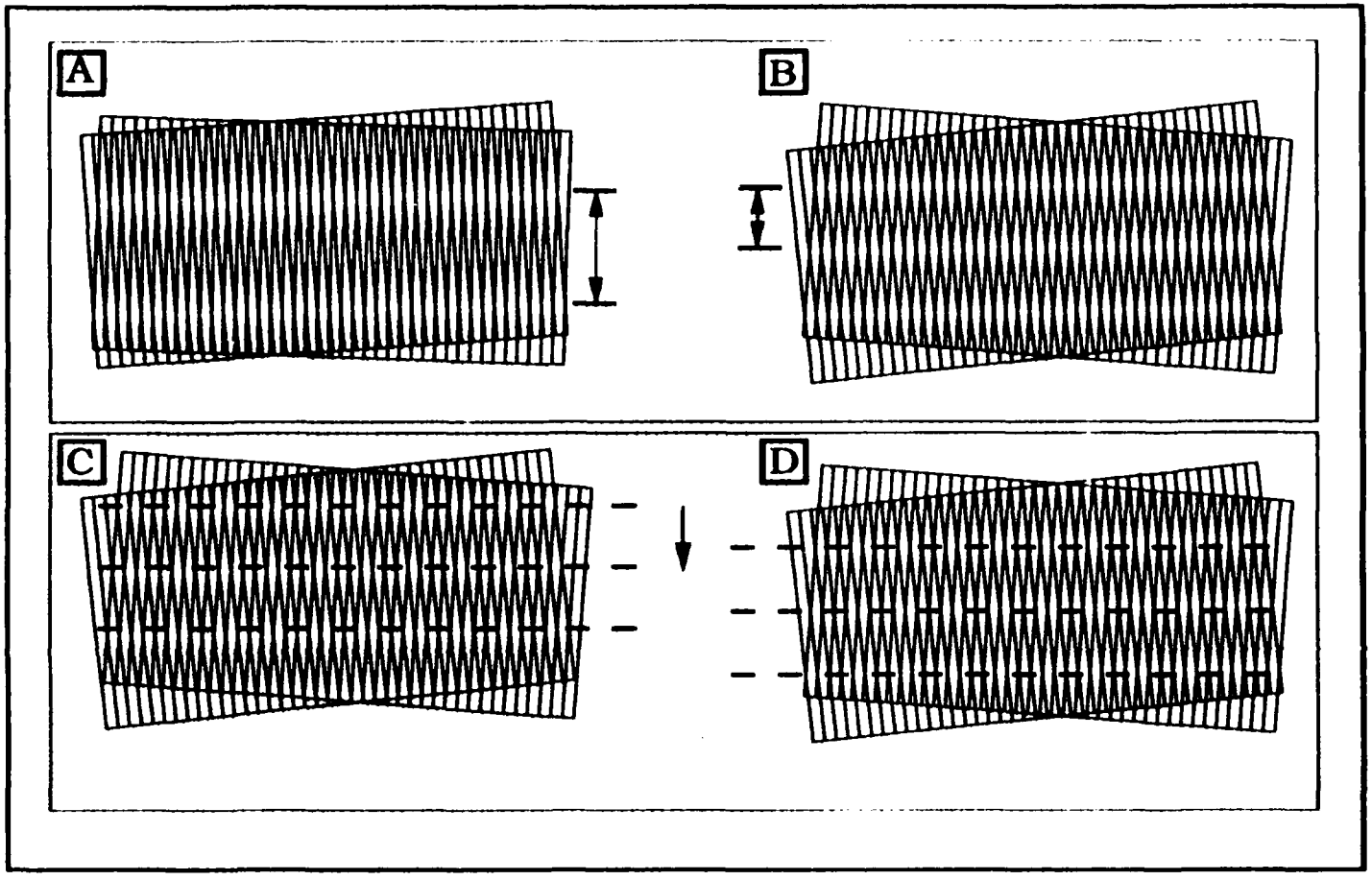

Figure 1

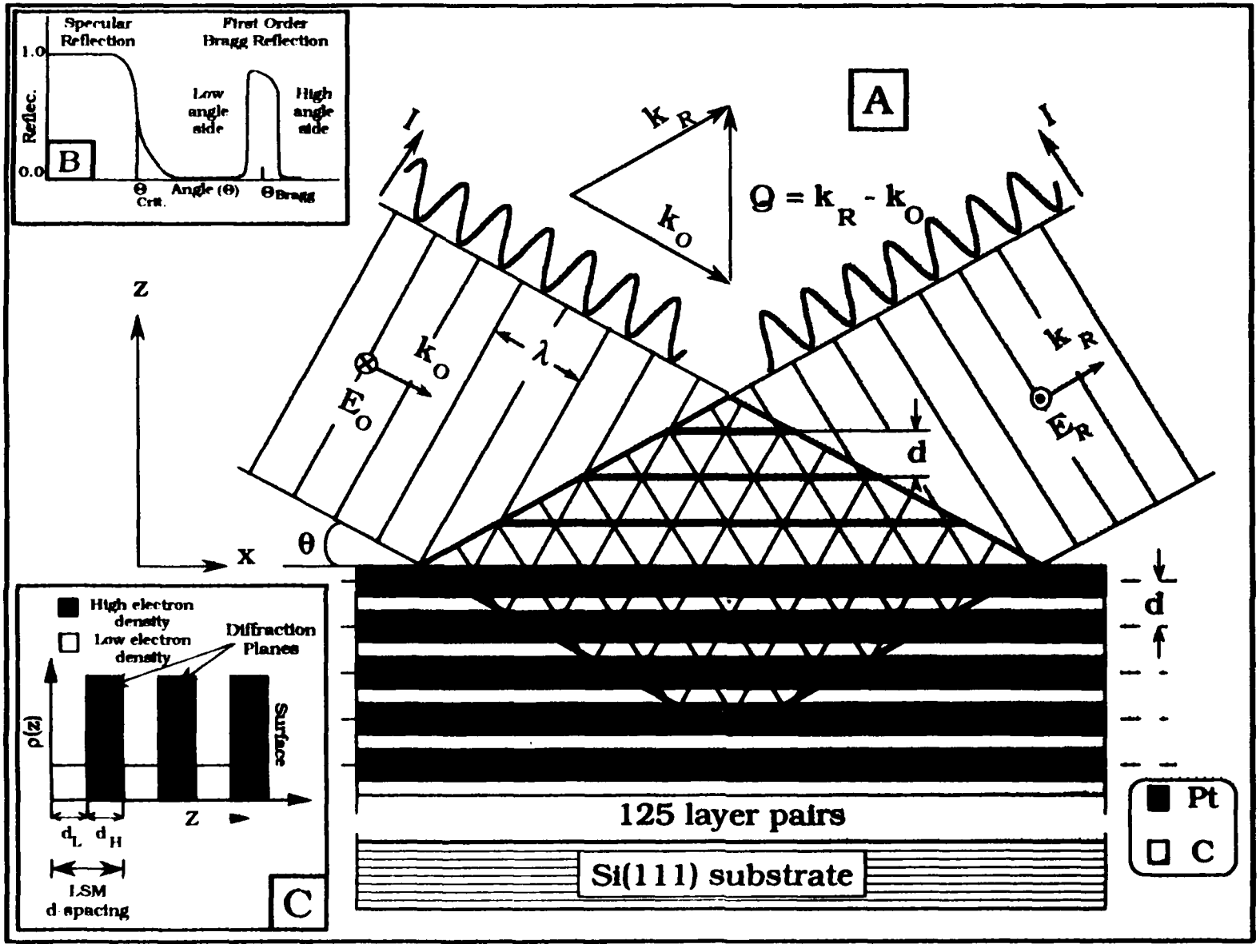
Specular Reflection
First Order Bragg Reflection
1.0
Reflec.
0.0
B
Low angle side
High angle side
Θ Crit.
Angle (Θ)
Θ Bragg
A
I
k R
k O
Q = k R - k O
Z
X
θ
E O
λ
d
E R
High electron density
Low electron density
Diffraction Planes
ρ(z)
Surface
d L
d H
LSM d-spacing
C
125 layer pairs
Si(111) substrate
Pt
C

Figure 2

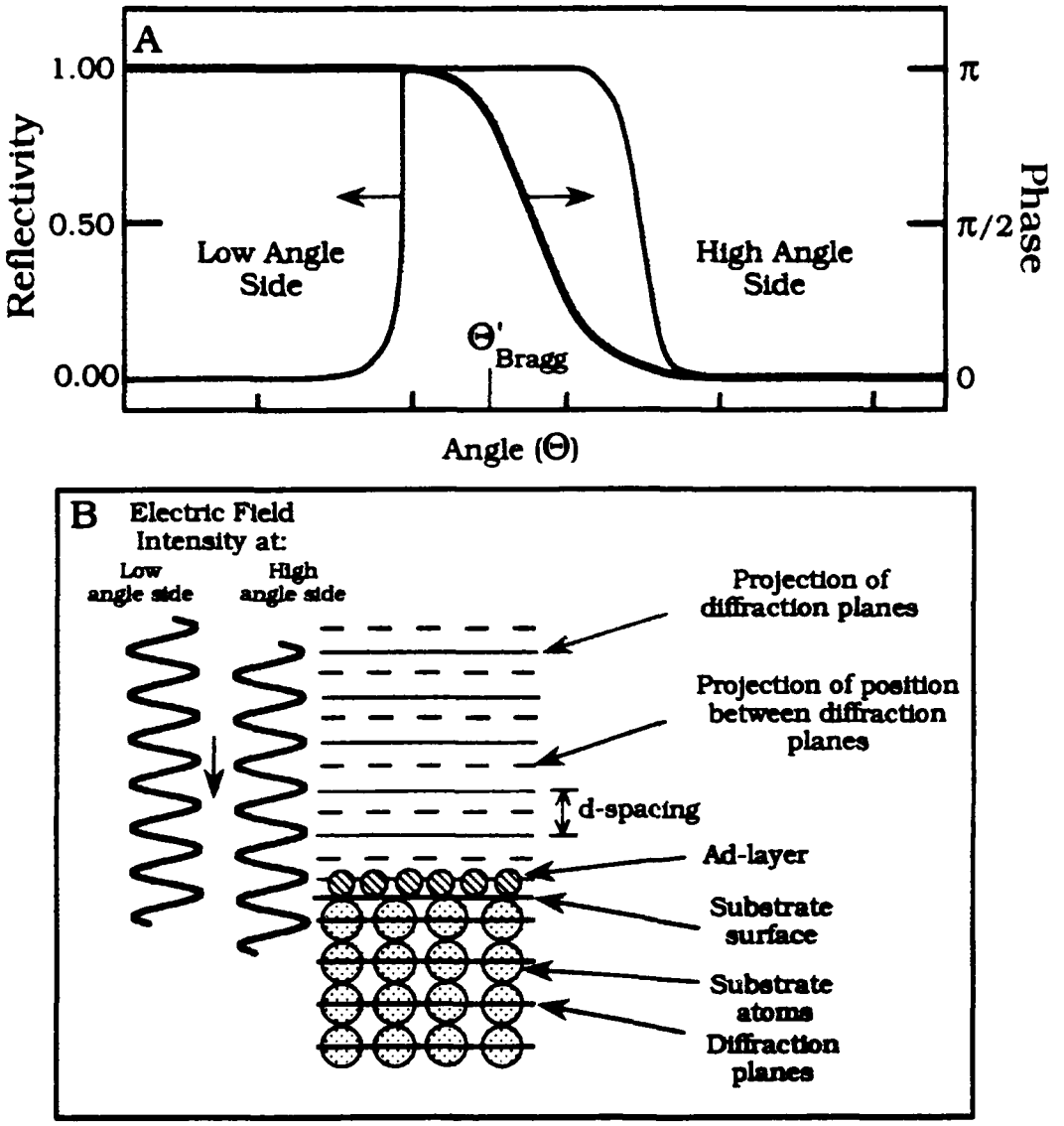
A
1.00
0.50
0.00
Reflectivity
π
π/2
0
Phase
Low Angle Side
High Angle Side
Θ'Bragg
Angle (Θ)
B
Electric Field Intensity at:
Low angle side
High angle side
Projection of diffraction planes
Projection of position between diffraction planes
d-spacing
Ad-layer
Substrate surface
Substrate atoms
Diffraction planes

Figure 3

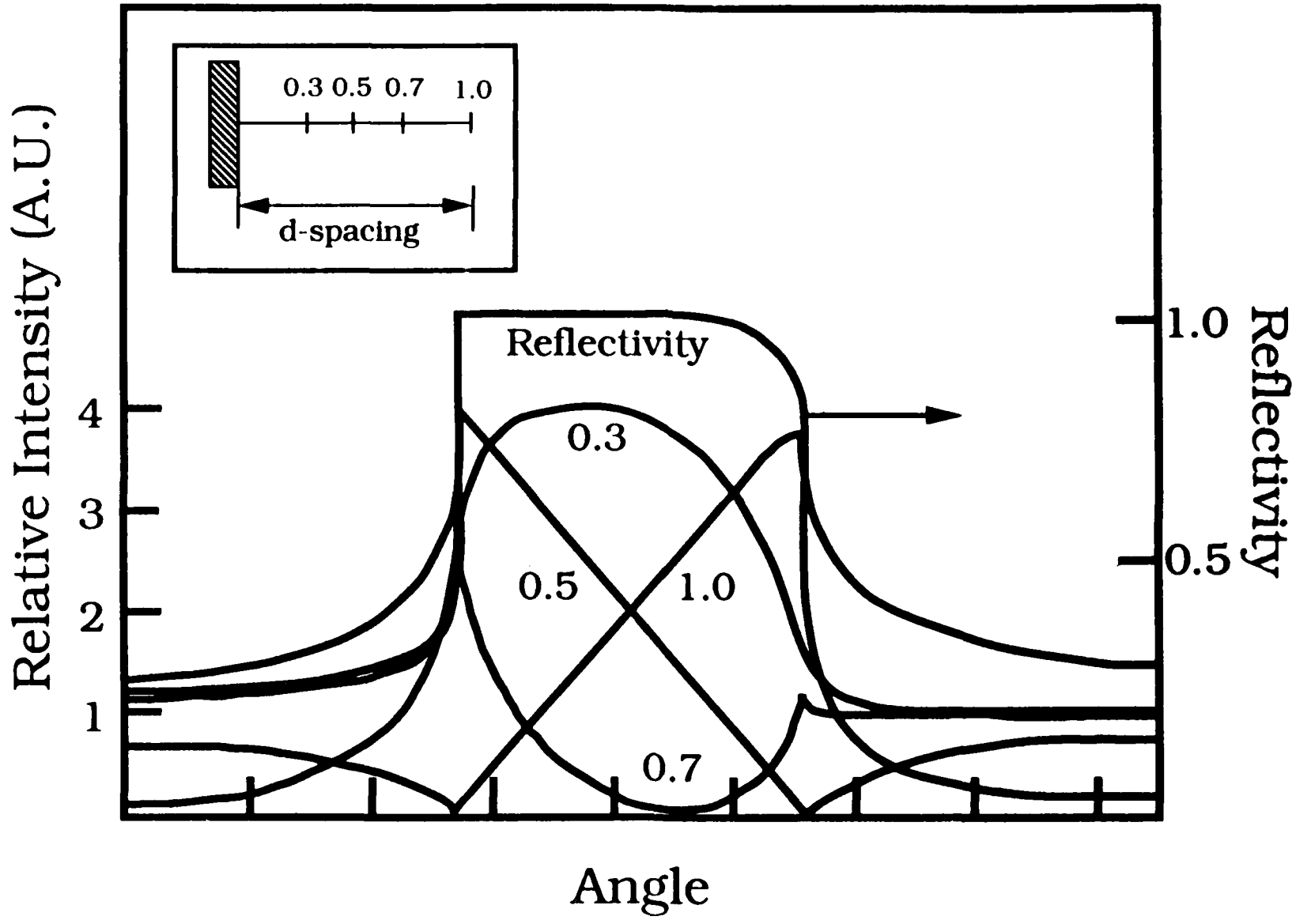
0.3 0.5 0.7 1.0
d-spacing
Reflectivity
0.3
0.5
1.0
0.7
Relative Intensity (A.U.)
4
3
2
1
1.0
0.5
Reflectivity
Angle

Figure 4

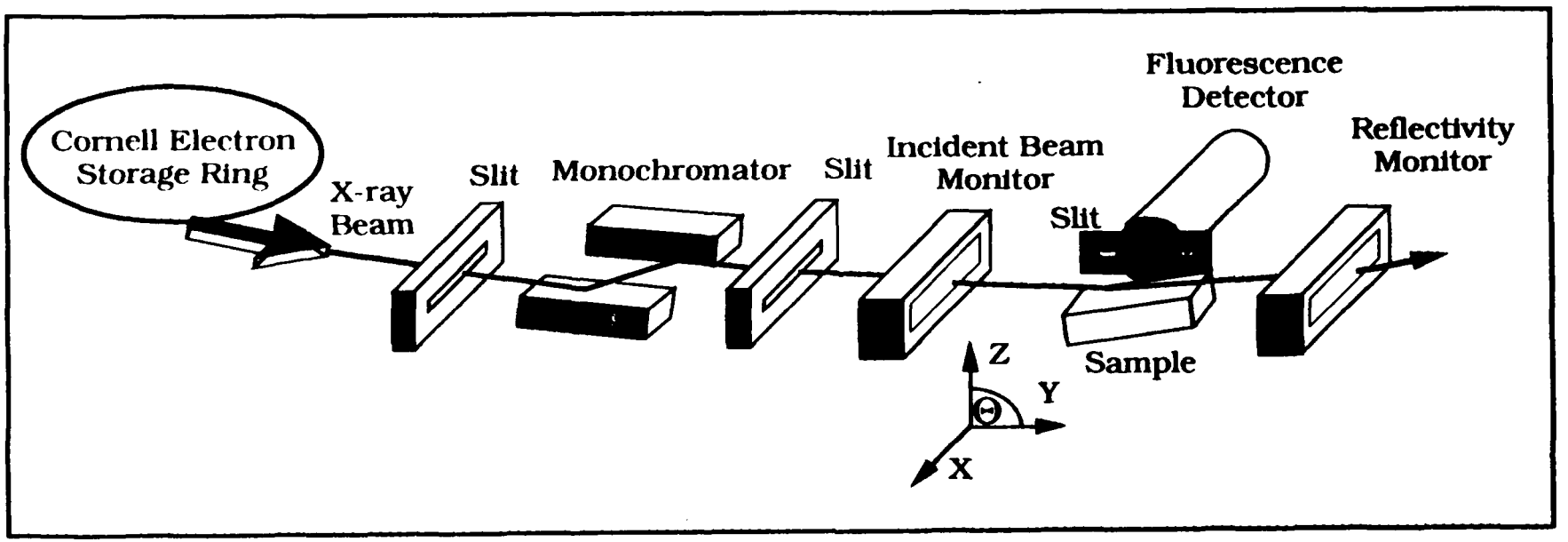
Cornell Electron
Storage Ring
X-ray
Beam
Slit
Monochromator
Slit
Incident Beam
Monitor
Slit
Fluorescence
Detector
Reflectivity
Monitor
Sample
Z
Y
X
Θ

Figure 5

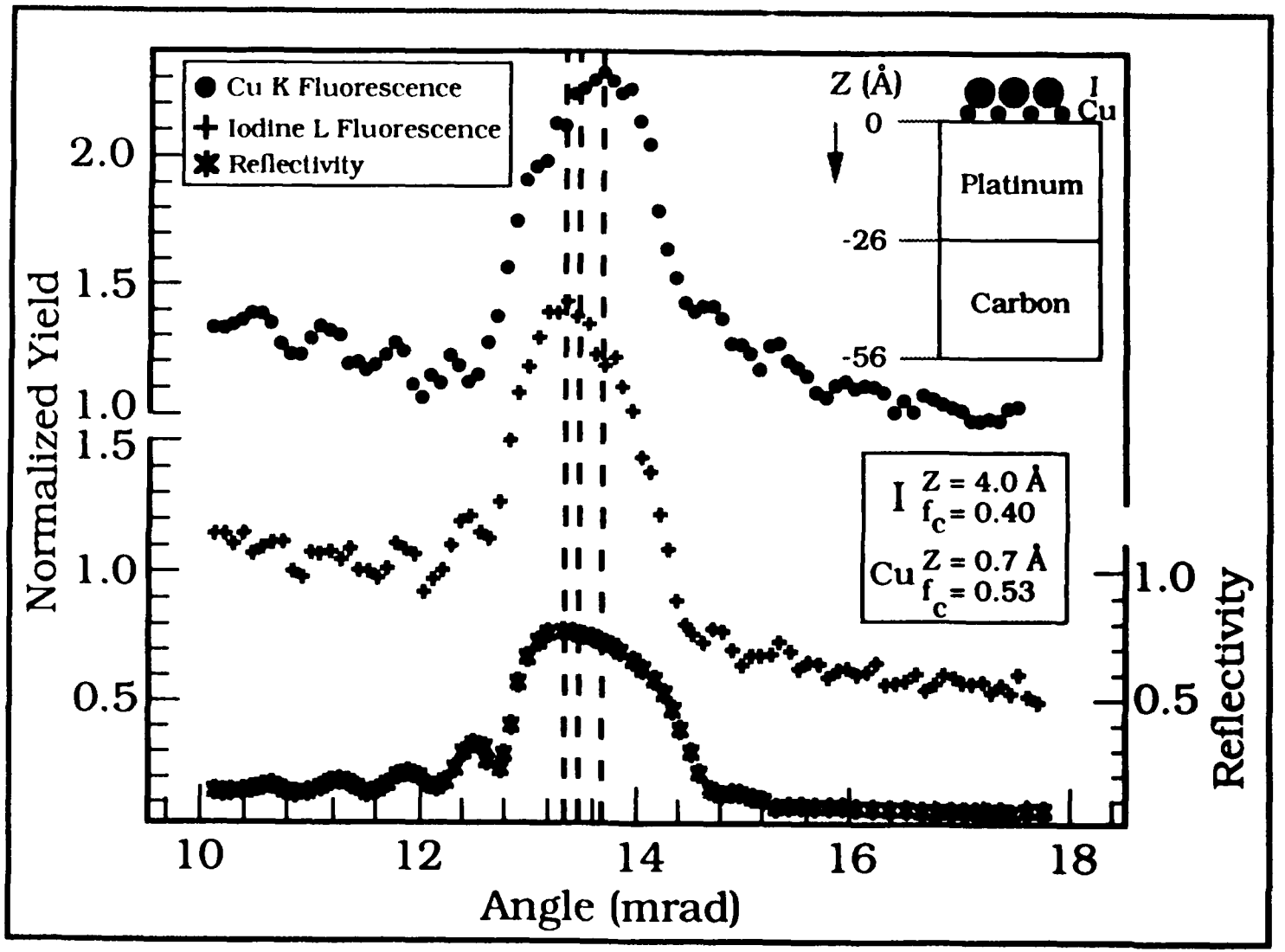
Cu K Fluorescence
Iodine L Fluorescence
Reflectivity
Z (Å)
0
-26
-56
I
Cu
Platinum
Carbon
I Z = 4.0 Å
f_c = 0.40
Cu Z = 0.7 Å
f_c = 0.53
Normalized Yield
2.0
1.5
1.0
1.5
1.0
0.5
1.0
0.5
Reflectivity
10
12
14
16
18
Angle (mrad)

Figure 6

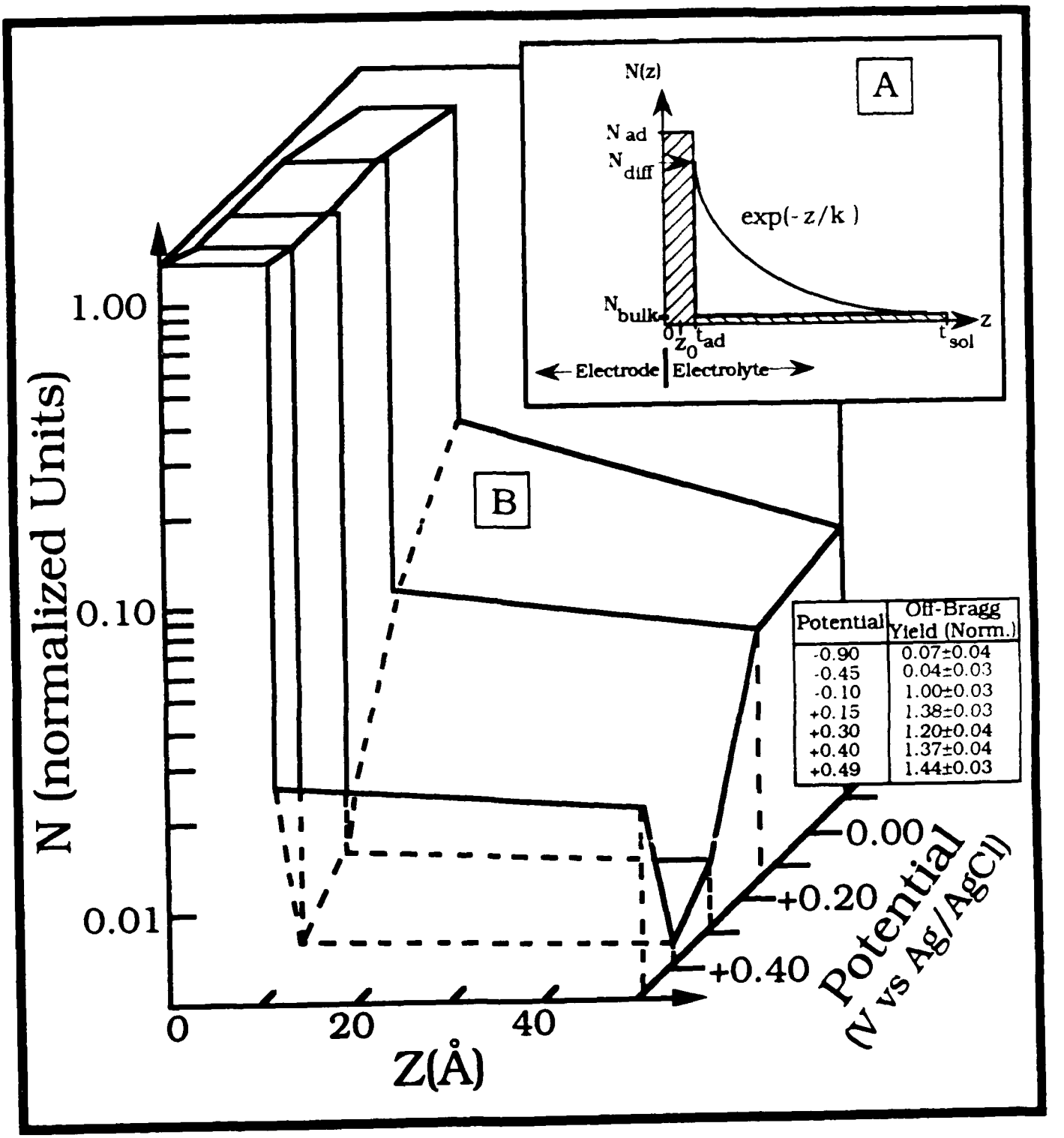
N(z)
A
N ad
N diff
exp(- z/k)
N bulk
0
z0
tad
tsol
z
Electrode
Electrolyte
B
1.00
0.10
0.01
N (normalized Units)
0
20
40
Z(Å)
0.00
+0.20
+0.40
Potential
(V vs Ag/AgCl)
Potential
Off-Bragg Yield (Norm.)
-0.90 0.07±0.04
-0.45 0.04±0.03
-0.10 1.00±0.03
+0.15 1.38±0.03
+0.30 1.20±0.04
+0.40 1.37±0.04
+0.49 1.44±0.03

Figure 7

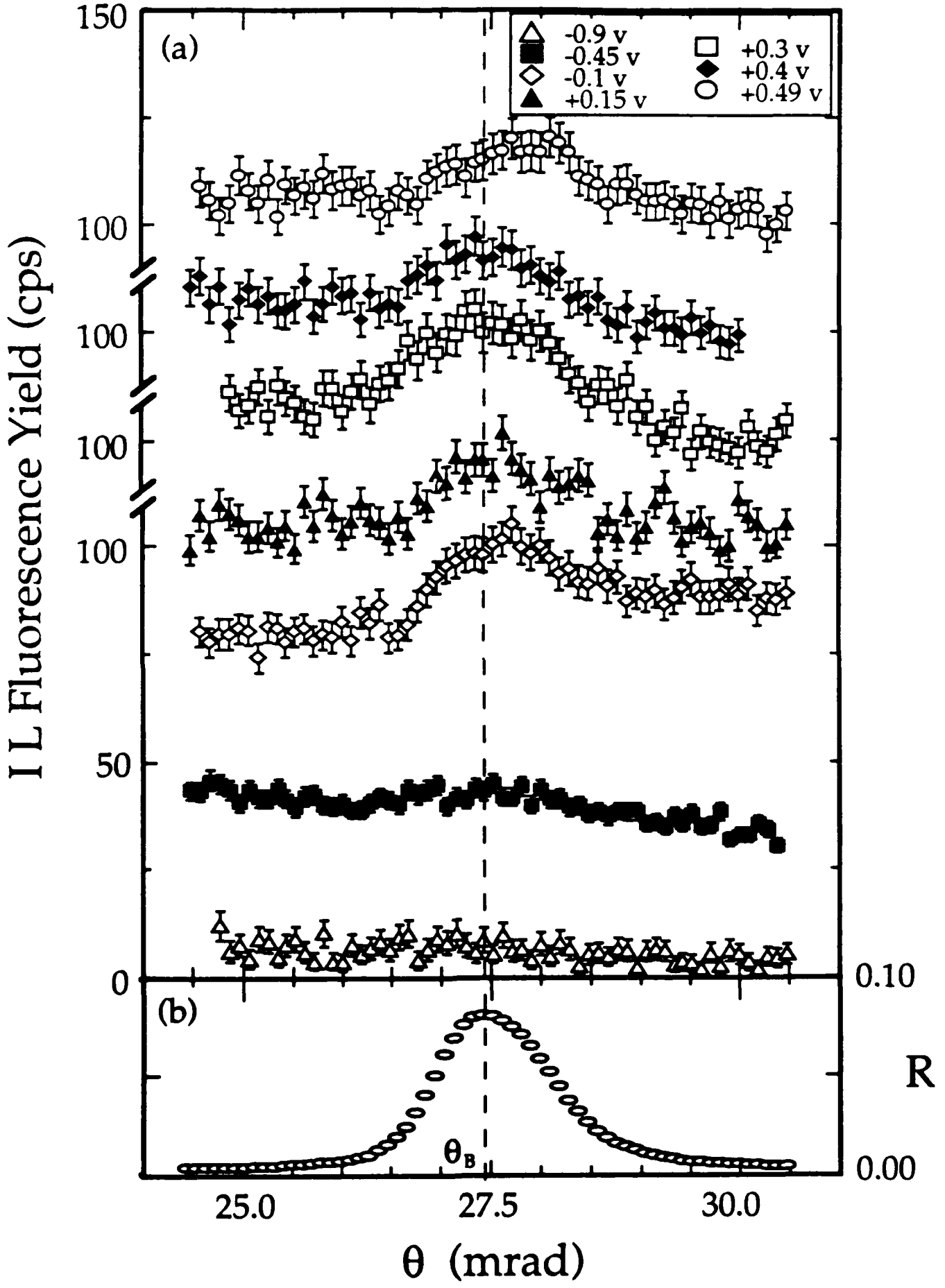
(a)
-0.9 v
-0.45 v
-0.1 v
+0.15 v
+0.3 v
+0.4 v
+0.49 v
150
100
100
100
50
0
I L Fluorescence Yield (cps)
(b)
0.10
0.00
R
θB
25.0
27.5
30.0
θ (mrad)

Figure 8

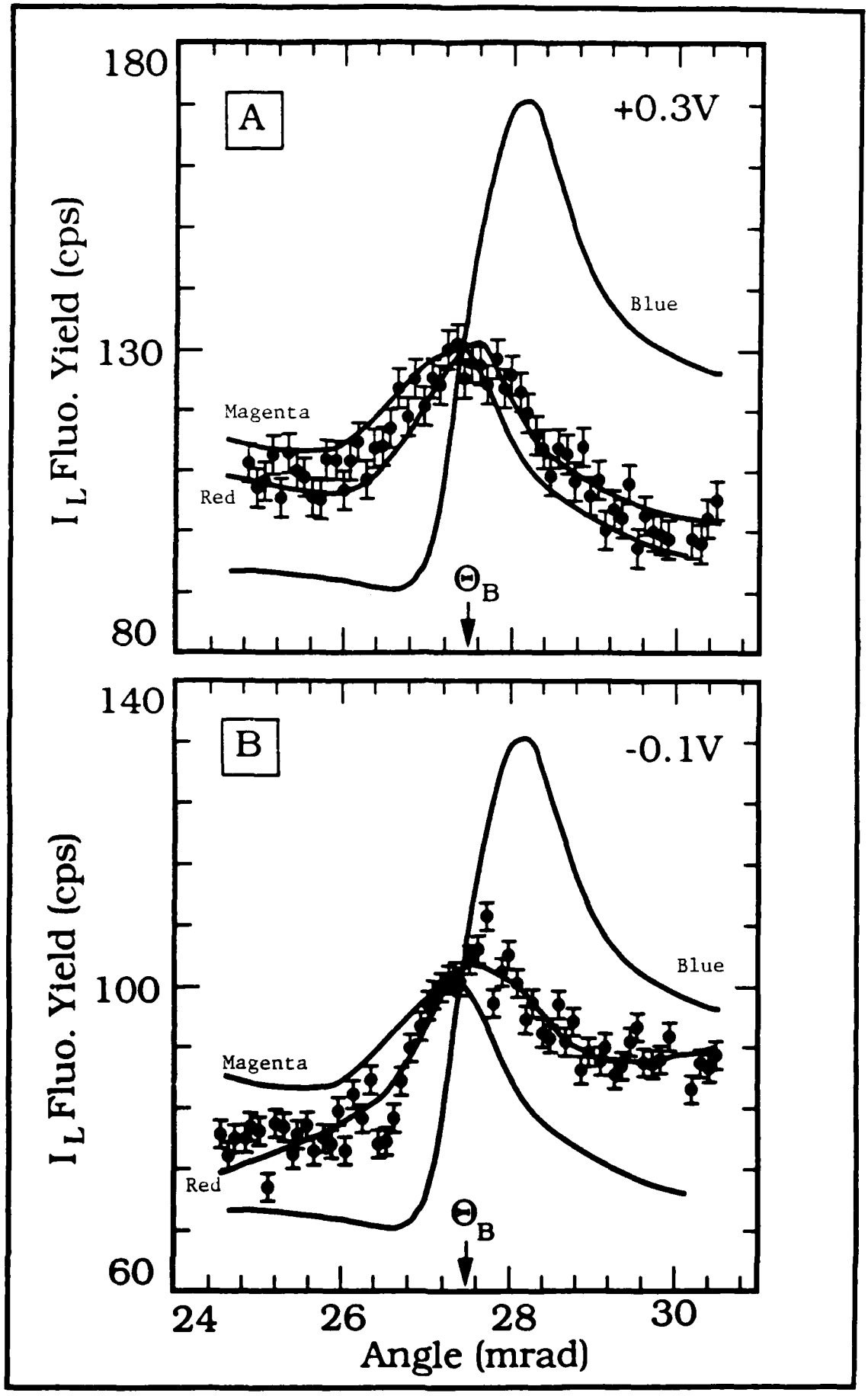
180
130
80
A
+0.3V
Blue
Magenta
Red
Θ_B
I_L Fluo. Yield (cps)
140
100
60
B
-0.1V
Blue
Magenta
Red
Θ_B
I_L Fluo. Yield (cps)
24
26
28
30
Angle (mrad)

Figure 9

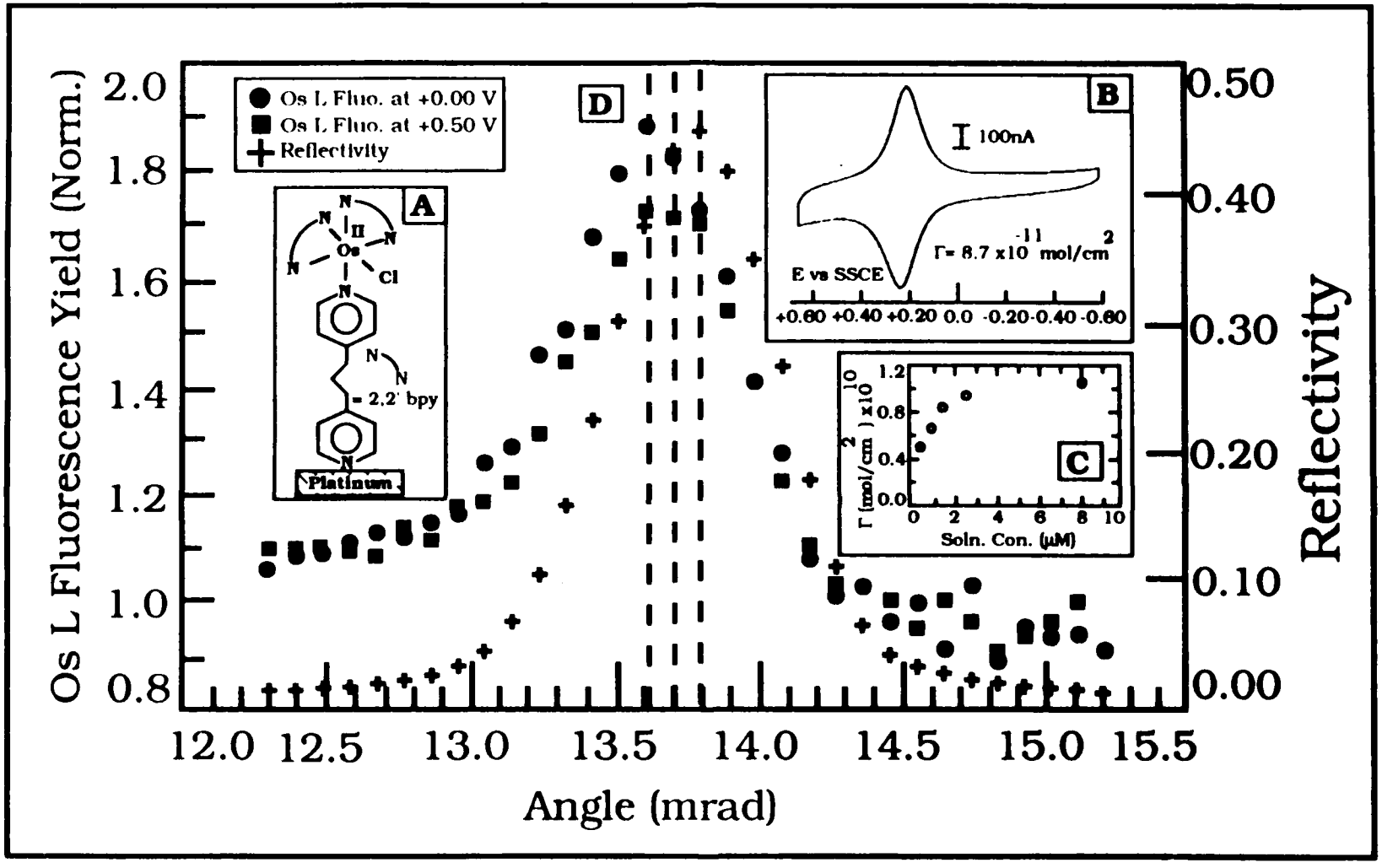
Os L Fluo. at +0.00 V
Os L Fluo. at +0.50 V
Reflectivity
D
A
Cl
= 2,2' bpy
Platinum
B
I 100nA
E vs SSCE
+0.60 +0.40 +0.20 0.0 -0.20 -0.40 -0.60
C
Soln. Con. (μM)
Os L Fluorescence Yield (Norm.)
Reflectivity
Angle (mrad)
2.0
1.8
1.6
1.4
1.2
1.0
0.8
0.50
0.40
0.30
0.20
0.10
0.00
12.0 12.5 13.0 13.5 14.0 14.5 15.0 15.5

Figure 10

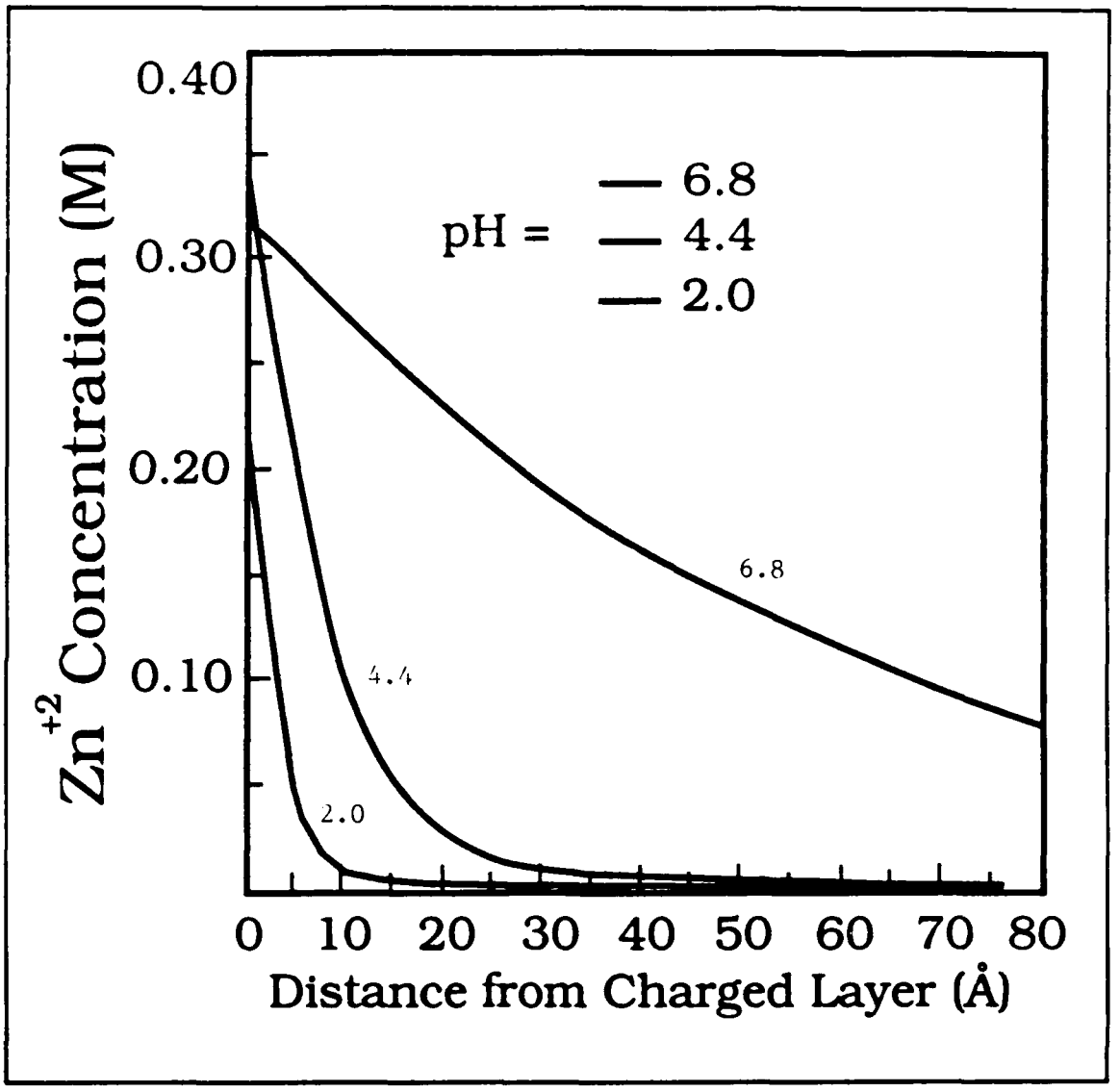
0.40
0.30
0.20
0.10
Zn^{+2} Concentration (M)
pH =
6.8
4.4
2.0
6.8
4.4
2.0
0 10 20 30 40 50 60 70 80
Distance from Charged Layer (Å)

Figure 11